International Journal of Nanomedicine

Dovepress
open access to scientific and medical research

Open Access Full Text Article

ORIGINAL RESEARCH

Tumor Microenvironment Multiple Responsive Nanoparticles for Targeted Delivery of Doxorubicin and CpG Against Triple-Negative Breast Cancer

Fenfen Gu[1,*], Chuling Hu[2,*], Wei Cao[3,*], Chao Li[1], Qingming Xia[4], Yuan Gao[4], Yan Liu[1], Shen Gao[1,4]

[1]Department of Clinical Pharmacy, Xinhua Hospital Affiliated to Shanghai Jiaotong University School of Medicine, Shanghai, People's Republic of China; [2]Jiaxing Maternity and Child Health Care Hospital, Jiaxing, People's Republic of China; [3]Department of Neurovascular Disease, Shanghai Fourth People's Hospital, School of Medicine, Tongji University, Shanghai, People's Republic of China; [4]Department of Pharmacy, Changhai Hospital, Second Military Medical University, Shanghai, People's Republic of China

*These authors contributed equally to this work

Correspondence: Shen Gao; Yan Liu, Tel/Fax +86 21 81873715; +86 21 25077156, Email liullk@126.com; liuyan03@xinhuamed.com.cn

Introduction: Currently, the main treatment for advanced breast cancer is still chemotherapy. Immunological and chemical combination therapy has a coordinated therapeutic effect and achieves some efficacy. However, the immunosuppressive tumor microenvironment is a major cause for the failure of immunotherapy in breast cancer. CpG oligodeoxynucleotides can activate the tumor immune microenvironment to reverse the failure of immunotherapy.

Methods: In this study, we designed an amphiphilic peptide micelle system (Co-LMs), which can targeted delivery of the immune adjuvant CpG and the chemotherapeutic drug doxorubicin to breast cancer tumors simultaneously. The peptide micelle system achieved tumor microenvironment pH and redox-sensitive drug release.

Results and Discussion: Co-LMs showed 2.3 times the antitumor efficacy of chemotherapy alone and 5.1 times the antitumor efficacy of immunotherapy alone in triple-negative breast cancer mice. Co-LMs activated cytotoxic CD8+ T lymphocytes and CD4+ T cells in mice to a greater extent than single treatments. We also found that Co-LMs inhibited the metastasis of circulating tumor cells in the bloodstream to some extent. These results indicate that the Co-LMs offer a promising therapeutic strategy against triple-negative breast cancer.

Keywords: chemo-immunotherapy, tumor microenvironment, CpG, nanoparticles, triple-negative breast cancer

Introduction

Breast cancer is a serious threat to the health of women worldwide.[1] Triple-negative breast cancer (TNBC), which has negative ER/PR/HER2 receptor expression, is the most malignant type of breast cancer with the worst prognosis, and patients with TNBC are unable to undergo endocrine and anti-HER2 targeted therapy. At present, the main treatment for TNBC is chemotherapy with anthracycline or taxane drugs. However, chemotherapy has many problems such as toxic side effects and the development of drug resistance.[2,3] Immunotherapy such as CTLA-4 or PD-L1 antibody drugs has been used for a variety of tumors and has revolutionized the management of cancers.[4] Compared with traditional chemotherapy, tumor immunotherapy has the advantages of lower toxicity and fewer side effects.[4–9] However, clinical studies have shown that immunotherapy alone does not increase OS values in patients with metastatic TNBC compared with chemotherapy.[10] One of the most important reasons for the failure of immunotherapy for breast cancer is the immunosuppressive tumor microenvironment (TME), which inhibits the transport, infiltration and activation of T cell or NK cell leading to the failure of immunotherapy.[11] TME is composed of a variety of immune regulatory factors secreted by tumor cells, stromal cells or immune cells responsible for intercellular communication, including cytokines, growth factors and chemokines.[12] Therefore, activating the tumor immune environment may stimulate the activity of killer

Received: 30 June 2022
Accepted: 25 August 2022
Published: 20 September 2022

T cells in vivo to achieve immunotherapy of breast cancer. Cytosine-phosphate-guanine (CpG) activates macrophages, dendritic cells and other immune cells by binding to TLR9 receptors on immune cell endosomes, stimulating them to secrete immune activation–stimulating factors, such as interleukin and tumor necrosis factor. Therefore, CpG is a very good immune adjuvant and has been the subject of intense study.[13,14] Reversing the immunosuppressive microenvironment by CPG is a strategy for immunotherapy of TNBC.

Recent studies have shown that chemo-immunotherapy has a dual effect on tumors: chemotherapy drugs kill tumor cells directly and also modulate the immune system by various mechanisms, releasing immune stimulators to restart the normal immune response to fight tumors.[15] At the same time, immunotherapy enhances the sensitivity of chemotherapeutic drugs and reduce drug resistance and systemic toxicity.[16] This combination in chemo-immunotherapy effectively kills tumor cells and promotes the reconstitution of the autoimmune system with low-toxic side-effects and long-acting anti-cancer effects.[17–19] The combination of chemotherapy and immunotherapy has achieved a good clinical effect in the clinical treatment of multiple types of tumors[5,8] and is one of most effective therapy against malignant tumors.[20–22] However, chemotherapeutic drugs and immune-drugs cannot usually be administered at the same time because of their different physical properties, which greatly reduces the synergistic efficacy. In addition, the distribution of chemotherapeutic drugs and immune-drugs in non-tumor sites leads to serious toxicity and off-target effects. Therefore, to obtain better efficacy of combination therapy, the development of a drug delivery system that takes into account the characteristics of these drug is critical.[23,24]

With the development of biomaterial research, it provided a good feasibility for the synergistic delivery of chemotherapy drugs and immune-adjuvant to achieve tumor targeting.[25,26] Polypeptide is a kind of compound with amino acids as the constituent unit. Peptides have attracted great interest in drug delivery systems.[27,28] The functional groups on peptides and the physical shape/size of peptide nanostructures have an important impact on the drug loading performance and carrier toxicity of nanoparticles. CpG is an oligonucleotide drug that needs to be transfected with a vector to help it escape from the lysosome when it enters the cell. We previously achieved lysosomal escape of CPG through the synthesis of a cell-penetrating peptide and verified that it has anti-tumor immune efficacy.[13] We also synthesized a smart vector that can coordinate DOX and nucleotide drugs to reach the tumor site and achieve lysosomal escape for nucleotide drugs. In addition, the carrier material is degraded in the tumor microenvironment.[29–32] The purpose of this study is to develop a more effective and accurate combination therapy of adriamycin and CPG. In this study, we modified our cell penetrating peptide and constructed a multifunctional nanomicelle. The nanomicelle uses a cationic carrier micellar chain with arginine-histidine-lipoics acid (LH_3R_6) to link CpG oligonucleotides. DOXO-EMCH connected with lipoic acid by hydrazone bond to form another micellar chain. Finally, lipophilic groups of lipoic acid were cross-linked and assembled to form stable nanomicelles (co-LMs). The nanomicelles carry the chemotherapeutic drug DOX and the immune adjuvant CpG to the tumor site and release DOX in tumor microenvironment in a pH-sensitive manner. CpG is protected from lysosomes and the carrier materials are eventually degraded in the glutathione-rich tumor microenvironment. The nanomicelles were associated with reduced leakage of DOX and CpG in the blood circulation. Our results indicate that nanomicelles represent a drug delivery system that is pH-sensitive and redox-sensitive for targeting tumors. This study provides a new strategy for the treatment of metastatic TNBC and a possibility for the immunotherapy of "cold tumor".

Materials and Methods

Materials

The following materials and reagents used in this study: lipoic acid, L-histidine hydrochloride, and L-arginine (Sangon Biotech, Shanghai, China); 1-ethyl-3-(3-dimethylaminopropyl) carbodiimide (EDC) and N-hydroxysuccinimide (NHS) (Aladdin, Shanghai, China); DOXO-EMCH (MCE, NJ, USA); dithiothreitol (DTT) (Sigma-Aldrich, St Louis, MO, USA); NH2-PEG-COOH (polyethylene glycol modified y amino and carboxyl) (MW: 2000) (BO Biological Technology Co., Ltd., Jiaxing, China); 4,6-diamidino-2-phenylindole (DAPI) (Sigma-Aldrich, St. Louis, MO, USA); Cell Counting Kit-8 (Dojindo Molecular Technologies, Tokyo, Japan); Medium RPMI 1640, penicillin streptomycin solution (5 kU/

mL), and fetal bovine serum (FBS) (Life Technologies, Grand Island, NY, USA); and CpG (5′-tcgtcgttttcggcgcgcgccg-3′) and Cy-5-labeled CpG (InvivoGen, San Diego, CA, USA).

Cell Lines and Animals

RAW 264.7 cells (Institute of Biochemistry and Cell Biology, Shanghai, China) were grown in DMEM supplemented with 10% FBS and antibiotics (100 U/mL penicillin and streptomycin). TNBC 4T1 cells (Institute of Biochemistry and Cell Biology, Shanghai, China) were grown in RMPI 1640 supplemented with 10% FBS and antibiotics (100 U/mL penicillin and streptomycin).

Female BALB/c nude mice, aged 6 weeks and weight 18–20 g (Second Military Medical University Animal Care Center, Shanghai, China), were maintained under specific pathogen-free (SPF) conditions. All animal experiments were conducted in accordance with the National Institutes of Health Guide for the Care and Use of Laboratory animals.

Synthesis of LH_3R_6-DOX-CpG Nanomicelles (Co-LMs)

The nanomicelles were synthesized in three steps. First, LA-PEG-DOX was synthesized. A 50 mg lipoic acid was dissolved in 0.5 mL methanol solution and then 50 mg EDC and 50 mg NHS were added and then the reaction was stirred for 6 h in the dark to activate the carboxyl group of LA. The unreacted EDC and NHS were removed by ultrafiltration and then 150 mg HS-PEG-NH2 was added, followed by stirring for 24 h in the dark. Then, 80 μL DOX-EMCH was added and the sample was stirred for 4–6 h. Unreacted impurities were removed by ultrafiltration, and methanol was dried with nitrogen to obtain LA-PEG-DOX chain.

Second, the DOX nanomicelles (DOX-LMs) were synthesized. The synthesis of the cationic cell-penetrating peptide LH_3R_6 was carried out according to previous studies.[13,30–32] LH_3R_6 and LA-PEG-DOX were co-dissolved in 1 ml methylene chloride; DTT was added, and the lipoic acid was cross-linked after 24 hours of mixing in dark. For phacoemulsification, 4 mL water was added (400W, 1 min/3 times) and then dispersed in the stirred water. After volatilization of methylene chloride for 12 h, the nanomicellar solution was obtained by ultrafiltration and purification, dried by lyophilization, and stored for further use. The DOX-LMs nanopolymer were also verified by ^{1}H-NMR at 600 MHz (Varian Inc., Palo Alto, CA, USA) in deuterium oxide. Finally, the DOX-CPG nanomicelles (Co-LMs) were synthesized. An appropriate amount of CpG was added to DOX-LMs vortexing for 30s at room temperature and incubating for 30 min to prepare Co – LMs before use.

Characterization of Co-LMs

The size and zeta potential were measured by dynamic light scattering method (DLS, Zetasizer Nano ZS90, Malvern, Worcestershire, UK). DOX-LMs were mixed with CpG at an N/P ratio of 1, 2.5, 5 and 10 with a total volume of 1 mL. The morphology of Co-LMs was confirmed by TEM (Hitachi, Tokyo, Japan), with an acceleration voltage of 75 kV. In addition, gel electrophoresis experiments were carried to verify the nucleotide compression ability of nanomicelles on CpG.

The pH-sensitivity of the drug release of Co-LMs was determined using a fluorescence detector (GloMax-Multi Jr Single Tube Multimode Reader). To detect pH sensitive drug release, 10% Co-LM solution was treated with disodium hydrogen phosphate citrate buffer at pH 5.5 or pH 7.4 and fluorescence value of DOX were detected at specific intervals.

Cell Uptake and Localization

To investigate the uptake of nanomicelles taken up by immune cells and tumor cells and the intracellular distribution, RAW 264.7 cells and 4T1 cells were, respectively, seeded in 12-well plates (1.5×10^5 cells/well) and grown for 24 h at 37 °C and 5% CO_2. To observe the uptake of CpGs by immune cells, we fluorescently labeled CpGs with FAM and treated 264.7 cells with PBS, lipo2000-CpG, or CpG-LMs (N/P=10) (CpG 100 nM) for 4 h. Flow cytometry was used to quantitatively detect the amount of cellular uptake.

Confocal laser scanning microscopy (CLSM) was also used to analyze the cellular localization. RAW264.7 cells were seeded in chambered coverslips (5×10^4 cells/well) in 24-well plates and grown for 24 h. Cells were treated with PBS, lipo2000-CpG, and CpG-LMs (N/P=10) (CpG 100 nM) for 4 h. Then, the medium was removed and samples were

washed with PBS three times and fixed with paraformaldehyde for 30 min. The nuclei were labeled with Hoechst and lysosomes were labeled with Giemsa staining solution. The cells were observed with confocal laser scanning microscopy (Nikon, Tokyo, Japan). The same method was used to investigate the uptake of doxorubicin by tumor 4T1 cells, except that the cells were exposed to PBS, DOX, and DOX-LMs.

Cell Viability Assays

CCK-8 assay was used to evaluate the in vitro cytotoxicity of LMs. Briefly, 4T1 cells were seeded in 96-well plates (8×10^3 cells/well) overnight. The cells were then exposed to serial concentrations (0–960 μg/mL) of the LMs and then incubated for 24 or 48 h. 10 μL of CCK-8 solution was added each well incubated for another 1 h after cleaning the culture medium with PBS. The absorbance of each well was measured with a microplate reader (Thermo Scientific, Waltham, MA, USA) at 450 nm. Cell viability was expressed as a percentage relative to the absorbance of the untreated cells. The results were calculated as means ± SD from at least three independent experiments. The IC_{50} of DOX and DOX-LMs for 4T1 cells was also evaluated with a CCK-8 assay. The experimental method was the same as described above except that cells were treated with different concentrations of DOX.

We also used flow cytometry to verify the killing ability of our nanoparticles on 4T1 cells. 4T1 cells were seeded into 12-well plates (3×10^5 cells/well). Then, after 24h, lymphocytes were extracted from spleen of mice by lymphocyte extract to co-cultured with 4T1 cells. Meanwhile, cells treated with PBS, LMs, CpG-LMs (CpG 100 nM), DOX (0.5 μg/mL DOX), DOX-LMs (0.5 μg/mL DOX) or Co-LMs (CpG 100 nM, 0.5 μg/mL DOX) for 48 h. After the culture medium were discarded, 4T1cells were harvested, washed with ice-cold PBS, and then stained with Annexin V–FITC and propidium iodide (PI) for 15 min at room temperature in the dark. Apoptosis was analyzed by flow cytometry (FACSCalibur; BD Biosciences, UK).

Enzyme-Linked Immunosorbent Assay (ELISA)

Enzyme-linked immunosorbent assay (ELISA) kits (R&D System, Minneapolis, MN, USA) were used to detect the levels of tumor necrosis factor-alpha (TNF-α) and interleukin-6 (IL-6). RAW264.7 cells were seeded in 24-well plates (1×10^5 cells/well) and grown for 24 h. CpG and nonCpG (5 μM) was complexed with LMs at N/P of 10 and incubated for 30 min before use. Then, the medium was replaced by LMs, lipo2000-CpG, CpG-LMs, nonCpG-LMs or lipopolysaccharide (LPS 10 ng/mL) for 8 and 24 h. The medium was collected and centrifuged at 3000 rpm for 20 min and then the supernatant was collected. TNF-α and IL-6 were detected by ELISA following the manufacturer's instructions.

Reverse Transcription-Polymerase Chain Reaction (RT-PCR)

The levels of TNF-α and IL-6 mRNA were measured in RAW264.7 cells treated with LMs, lipo200-CpG, CpG-LMs, nonCpG-LMs and LPS (10 ng/mL)) (5 μM CpG). All of the RNA was extracted by TRIzol and treated with double DNase. RT-PCR was performed using the SuperScript® one-step RT-PCR with Platinum Taq (Invitrogen) following the manufacturer's protocol. The following primers were used: β-actin, 5′-ACT TCG AGC AGG AGA TGGCC-3′ (forward) and 5′-CCC AAG GAA GGC TGGAA-3′ (reverse); IL-6, 5′-CAC AAG TCC GGA GAGGAG AC-3′ (forward) and 5′-TCC ACG ATT TCC CAGAGA AC-3′ (reverse); and TNF-α, 5′-CGG CATGGATCT CAA AGA CA-3′ (forward) and 5′-ATA GCA AATCGG CTG ACG GT-3′ (reverse).

In vivo Distribution of LMs

Cy5 fluorescence was used to label nanoparticles Cy5-CpG-LMs (N/P=10) to explore the distribution of LMs in vivo. The absorbance of Cy5 was determined at 650 nm. A 0.1 mL 4T1 cell suspension (1×10^7 cells) was injected into the right flank of female BALB/c nude mice to establish the model of transplanted tumor in mice. Ten days post-inoculation, Cy5-CpG-LMs were injected through the tail vein at a single Cy5-CpG dose of 1 mg/kg (250 μL solution). The mice were euthanized at 30 min, 1 h, 2 h, 6 h, 12 h, or 24 h post-injection. The tumors, hearts, livers, spleens, lungs, and kidneys were extracted, washed in PBS, and scanned using the Bio-Real Quick View 3000 imaging system (Bio-Real Sciences, Vienna, Austria).

In vivo Antitumor Effects

To investigate the in vivo effects of Co-LMs, the BALB/c mouse model with 4T1 cells was used. The xenograft tumor model was established in the same way as before. Ten days after injection, the mice were randomly divided into six

groups (n=5 each group): (1) PBS, (2) LMs, (3) DOX, (4) DOX-LMs, (5) CpG-LMs, and (6) Co-LMs (5 mg/kg DOX and 1 mg/kg CpG). The mice were injected on days 0, 3, 6, 9, 12 and 15. Mice were euthanized on day 21. The tumors were measured with a caliper every three days. Tumor volume was calculated using the following formula: volume = length × width^2/2. In the end, the tumors were removed from the mouse and weighed.

Histological Analysis

Hematoxylin and eosin (H&E) staining were used to analyze the tumor histology, according to standard protocols.

After mice were euthanized, the tumor tissues were stripped and fixed with 4% paraformaldehyde for 24 h and then embedded in paraffin. Tissue sections (5 μm thick) were stained with H&E. Images of the stained histological specimens were captured using a Leica DM 1000 LED Microscope (Leica Microsystems, Cambridge, UK) equipped with a CDD digital camera (Qimaging, UK).

In vivo Immune Effect

After mice from the six groups were euthanized, the spleen was removed, and the lymphocytes were extracted by grinding with lymphocyte extract. The lymphocytes were stained with fluorescence-labeled antibodies (PE anti-mouse CD 3, APC anti-mouse CD8 and FITC anti-mouse CD4) on ice for 30 min and then washed with ice-cold PBS containing 0.1% NaN_3 and 0.5% BSA. Flow cytometry was used to detect $CD4^+$ and $CD8^+$ T-cells.

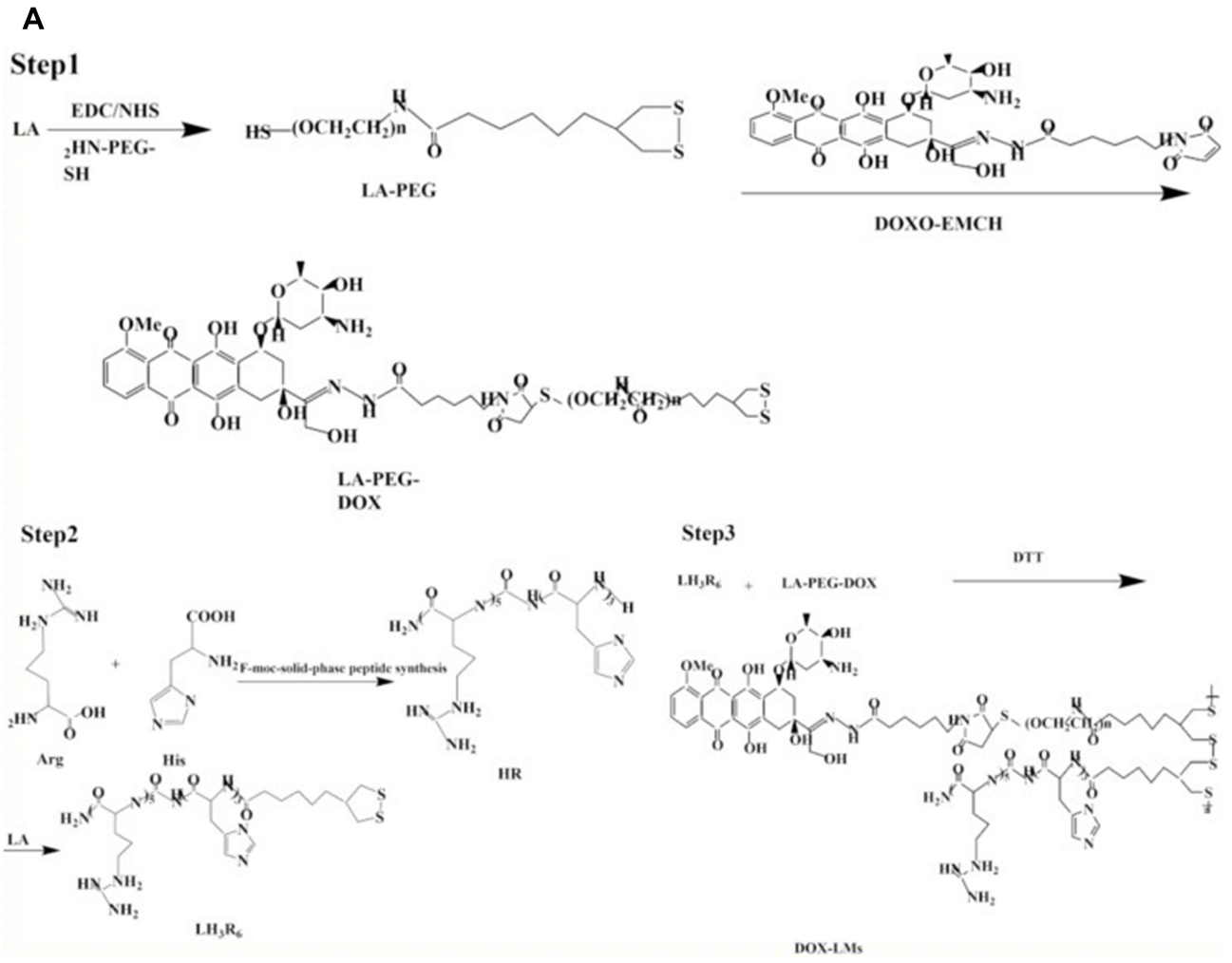

Figure 1 Continue.

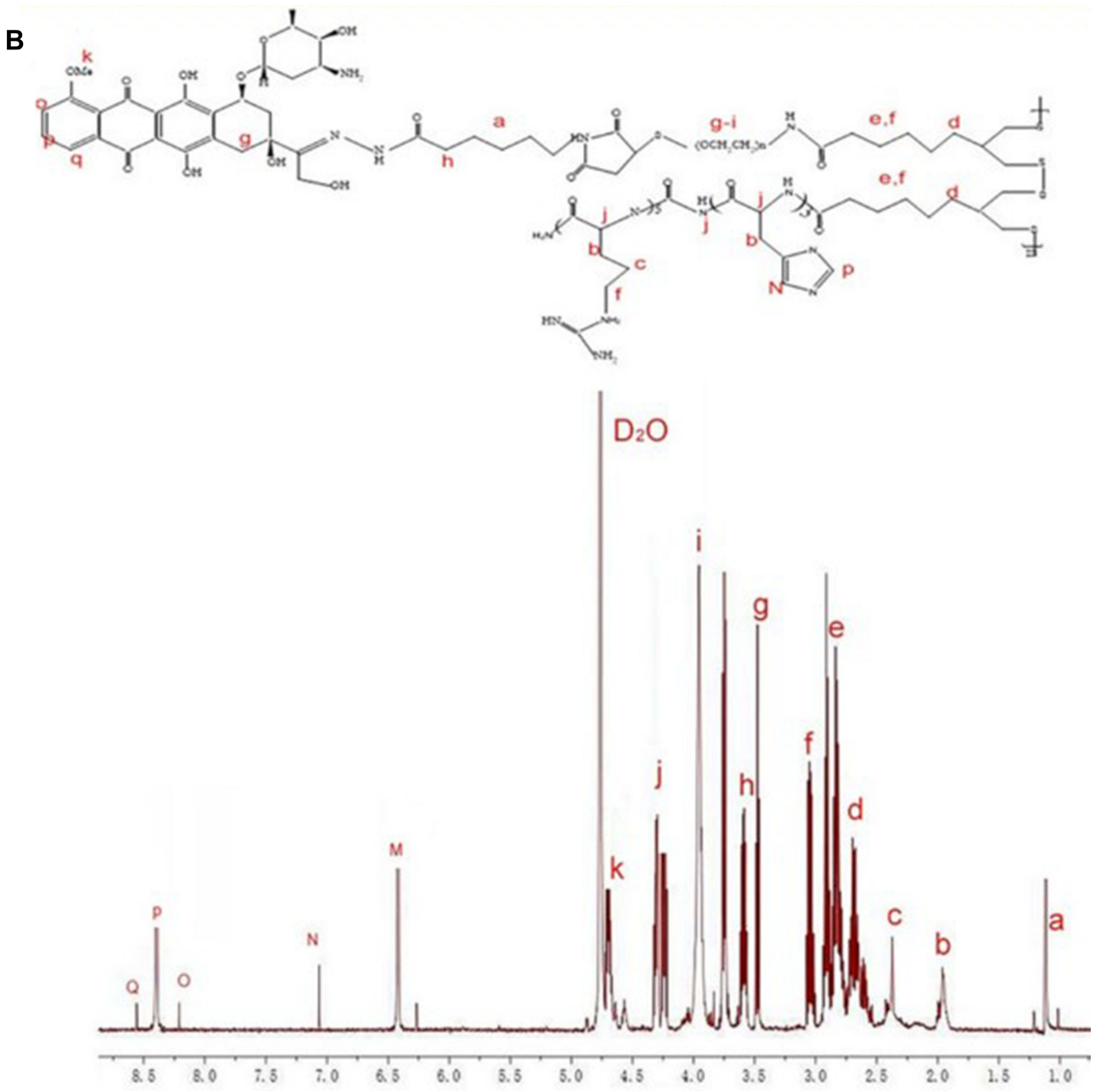

Figure 1 Synthesis and ^{1}H-NMR determination of MWCNT-H3R6 (MHR). (**A**) Synthesis of DOX-LMs and (**B**) ^{1}H-NMR spectra of DOX-LMs in D_2O at 600 MHz.

Anti-Hematogenous Metastasis Research

To explore the effects of treatment on circulating tumor cells in advanced tumors, the 4T1-luciferase cell suspensions (0.2 mL, 1×10^{6} cells/mL) were injected in 18 female BALB/c mice via the tail vein. Mice were divided into six groups (n=3 per group): (1) PBS, (2) LMs, (3) DOX, (4) DOX-LMs, (5) CpG-LMs, and (6) Co-LMs (5 mg/kg DOX and 1 mg/kg CpG). The mice were injected on days 0, 3, 6, and 9 after tumor cell injection on day 0 and tumor metastasis in the mice was observed on day 12 using an in vivo imaging system. The mice were then sacrificed and dissected, and the lungs were removed to examine tumor metastasis.

Statistical Analysis

Analysis of variance (ANOVA) was used for statistical analyses. Differences were considered statistically significant at $p < 0.05$. Results are shown as the mean ± SD.

Results and Discussion

Characterization of LMs

The main synthesis steps are shown in Figure 1A and the ^{1}H-NMR spectrum of DOX-LMs is shown in Figure 1B. The peaks at δ 1.05 ppm (signal a) were attributed to the –CH2-group of PEG. The peaks at δ 1.81 ppm (signal b), δ 2.37 ppm (signal c) and δ 3.11 ppm (signal f) were attributed to the –CH2-group adjacent to the secondary carbon of arginine. The signals at 4.25 ppm (signal j) were attributed to the tertiary carbon of histidine. The peaks at δ7.05 ppm (signal n) and δ 8.31 ppm (signal p) were from the protons of imidazole in histidine. All characteristic peaks are marked in the figure.

Transmission electron microscopy of the nanomicelles showed a regular spherical shape (Figure 2A) and the Co-LMs (DOX-CpG-nanomicelle (N/P =10)) had a mean size of 103 nm ± 8.25 nm and the mean zeta potential changed to 23.4 mV ± 1.56 mV after modification with CpG (N/P =10) (Figure 2B). The size and zeta potential of the Co-LMs were suitable for systemic administration which ensured that it has a good enhanced permeability and retention (EPR) effect.[33,34] The compression ability of polymer nanoparticles to CpG ODN was determined by agarose gel electrophoresis. As shown in Figure 2C, as the N/P ratio increases, the ability of micelles to compress nucleotides also increases. When the N/P ratio = 10, micelles can completely compress nucleotides. The DOX release process of the Co-LMs was researched at pH 5.5 or pH 7.4 at 37 °C. As shown in Figure 2D, nanomicelles are pH-sensitive for DOX release. At pH 5.5, the cumulative release of DOX from Co-LMs was approximately 86% within 48 h, while at pH 7.4, only approximately 27% was released. The reason for this release trend is mainly from the easy cleavage of the hydrazone bond between approximately pH 5.5–6.6[35,36]

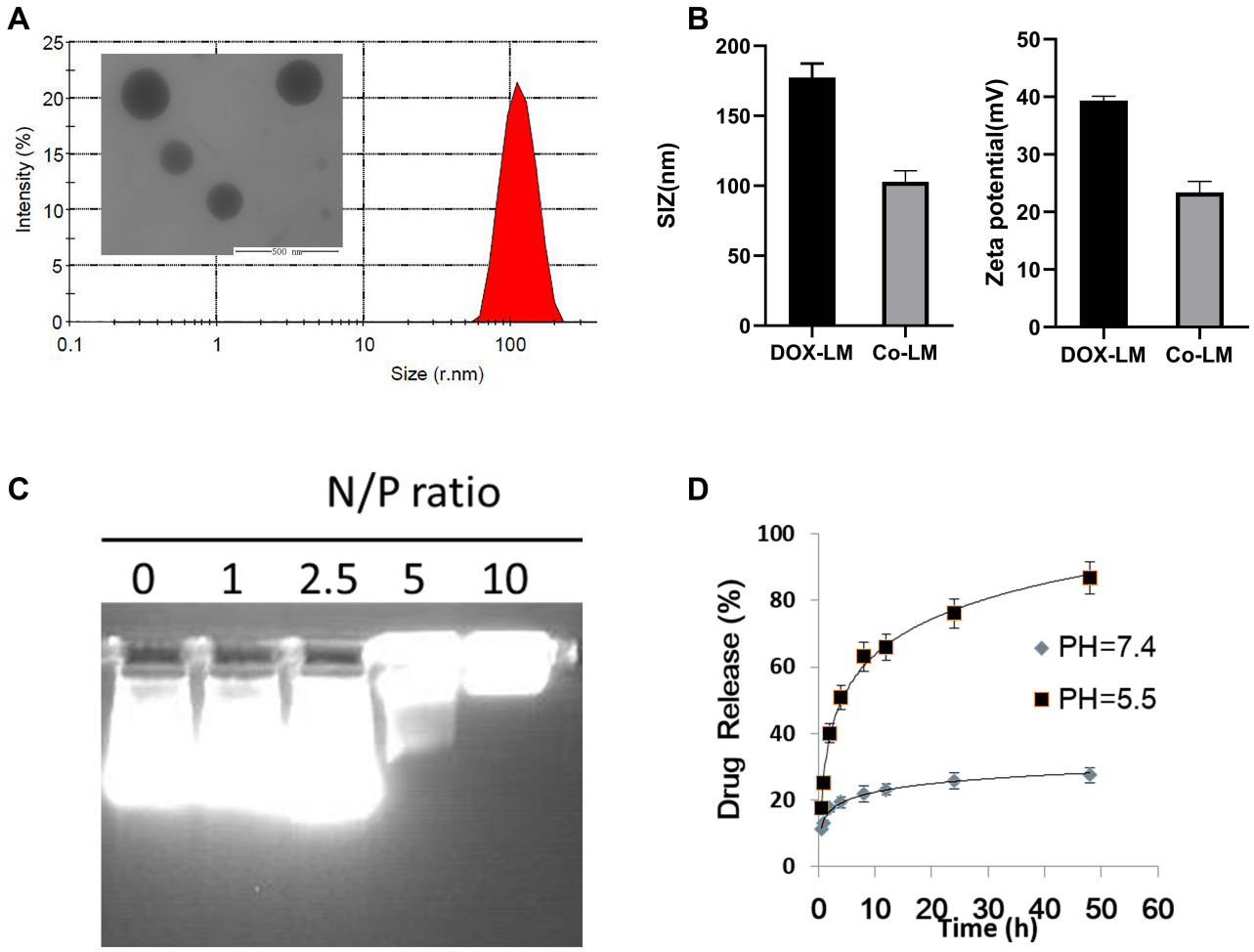

Figure 2 Characterization of Co-LMs. (**A**) TEM images and Particle size of Co-LMs. (**B**) Particle size and Zeta potential of Co-LMs and DOX-LMs. (**C**) Agarose gel electrophoresis results for Co-LMs. (D) The process of doxorubicin (DOX) release from Co-LMs in PBS at pH 5.5 or pH 7.4 at 37°C.

In vitro Cellular Uptake

The intracellular localizations of CpG and DOX were analyzed using confocal laser scanning microscopy in RAW264.7 cells and 4T1 cells, respectively. As shown in Figure 3A, in RAW264.7 cells, CpG distributed in cytoplasm. The CpG uptake in the CpG-LMs group was markedly higher than that in the lipo2000-CpG group, and most of the CpG in the CpG-LMs group escaped phagocytosis by lysosomes. This is mainly due to the proton sponge effect of histidine in our micelles.[13,30] To investigate the uptake of nanomicelles by immune cells tumor cells, flow cytometry and fluorescence confocal microscopy were used. Flow cytometry analysis showed a high level of CpG-LMs uptake compared with uptake of lipo2000-CpG, which demonstrated that nanoparticles significantly enhanced the uptake of CpG by RAW264.7 cells (40.7% vs 72.3%, $p<0.01$) (Figure 3B and C).

To examine the vitro cellular uptake by tumor cells, 4T1 cells were cultured. In Figure 4A, DOX was observed to effectively enter the nucleus. Flow cytometry analysis showed that the uptake in the DOX-LMs group was close to that in the free DOX group. In 4T1 cells, the cellular uptake of free DOX and DOX-LMs was high (96.3% and 98.08%, $p>0.05$) (Figure 4B and C). The flow cytometry data was consistent with confocal results. These results suggest that our nanomicelles can carry CpG and DOX into the nucleus to exert their effects.

Cell Viability and Apoptosis

We used CCK-8 assays to first study the cytotoxicity of blank vector (LMs) on 4T1 cells. As shown in Figure 5A, the cell viability remained approximately >80% in cells treated with a high concentration of LMs (960 μg/ml) after 24 and 48 h of incubation, indicating that blank carrier materials had negligible cytotoxicity and good biocompatibility. As shown in Figure 5B, the cell viability was reduced after treatment with DOX, DOX-LMs at DOX concentrations of 0–2 μg/ml in a concentration-dependent manner. The IC_{50} values for free DOX and DOX-LMs against 4T1 cells at 48 h were 0.96 μg/

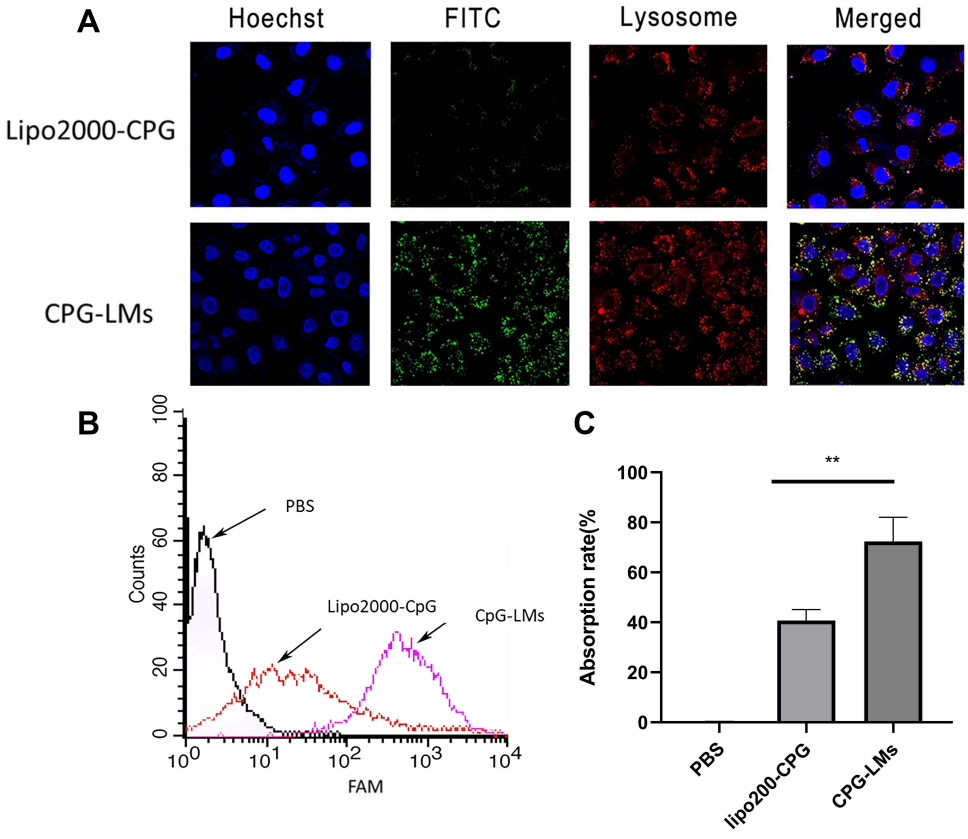

Figure 3 The cellular uptake of FITC-labeled CpG-LMs. (**A**) Confocal microscopic images of RAW264.7 cells incubated with CpG-LMs and Lipofectamine2000+CpG for 4 h. Green fluorescence presents FITC-labeled CpG, red fluorescence represents lysosome, and blue fluorescence represents the cell nucleus. Scale bar is 20 μm. (**B**) Flow cytometry figures of CpG-LMs and lipo2000-CpG uptake by RAW264.7 cells. (**C**) Quantitative analysis of the percentage of positive CpG cells. **p <0.01.

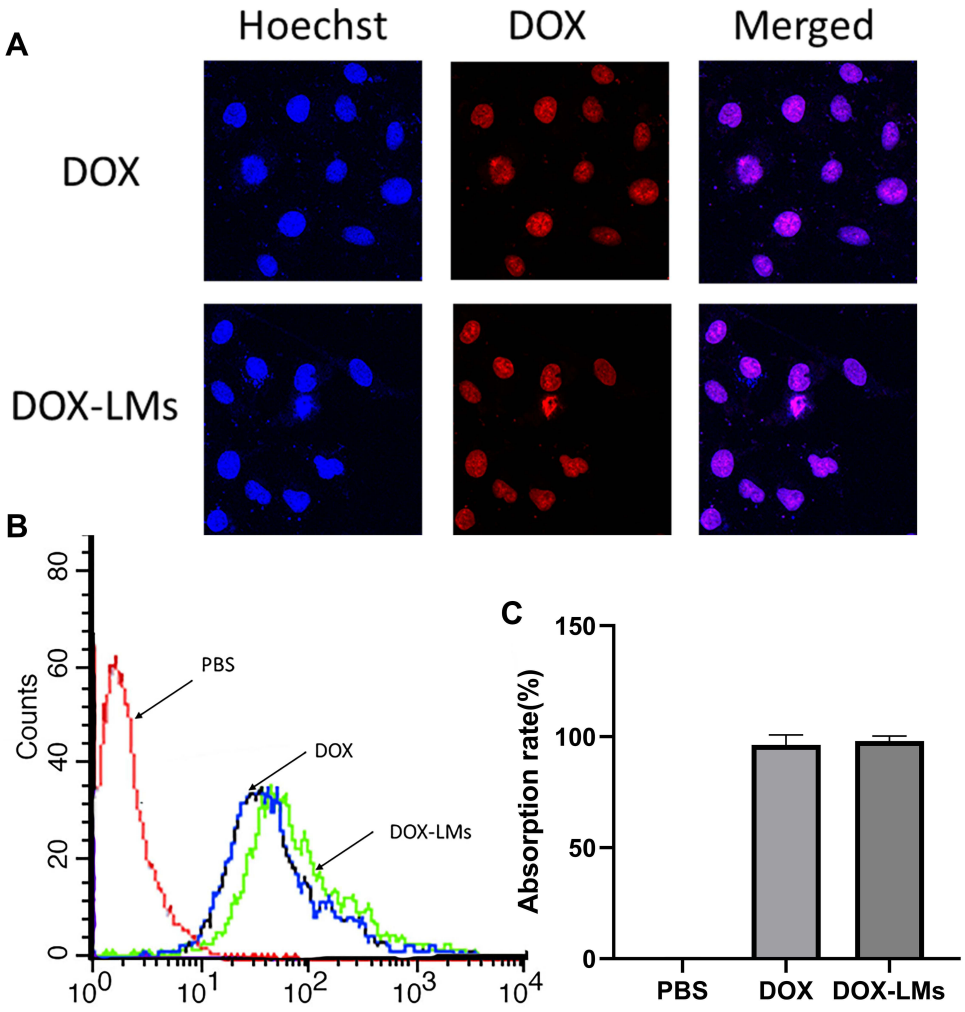

Figure 4 The cellular uptake of DOX-LMs. (**A**) Confocal microscopic images of 4T1cells incubated with DOX-LMs and free DOX for 4 h. Red fluorescence represents DOX, and blue fluorescence represents the cell nucleus. Scale bar is 20 μm. (**B**) Flow cytometry figures of DOX-LMs and free DOX uptake by 4T1 cells. (**C**) Quantitative analysis of the percentage of positive DOX cells.

mL (95% CI [0.8–1.13 μg/mL]) and 0.51 μg/mL (95% CI [0.42–0.64 μg/mL]). To evaluate the effects of Co-LMs on apoptosis in 4T1 cells, mouse lymphocytes were co-cultured with 4T1 cells and cell apoptosis was monitored by flow cytometry after staining with FITC-Annexin V/PI. As shown in Figure 5C, there were only a few apoptotic and dead cells in blank group and blank vector group. However, increased apoptosis was detected in Co-LMs group. In the Co-LMs group, 32.55% of cells were apoptotic compared with 19.34% in the DOX-LMs group, 16.98% in DOX group and 8.94% in CpG-LMs, which suggested that Co-loading group had better synergistic antitumor activity due to activation of immune cell. The reason for the good effect of co-LMs on promoting tumor apoptosis was the synergistic effect of DOX and CPG. In addition, due to the protonation of histidine in micelle structure, it will destroy the internal structure of micelles and further promote the release of DOX.[32]

Cytokine Test in vitro

The TNF-α and IL-6 cytokines induce Th1/2 differentiation and CpG induces the Th1 type immune response, producing strong humoral and cellular immunity and enhancing specific and non-specific immune responses.[23] To study the effect of CpG-LMs on both humoral and cellular immune responses, we examined the secretion levels of these cytokines. As shown in Figure 6A, treatment with CpG-LMs resulted in increased TNF-α and IL-6 to a higher extent compared with

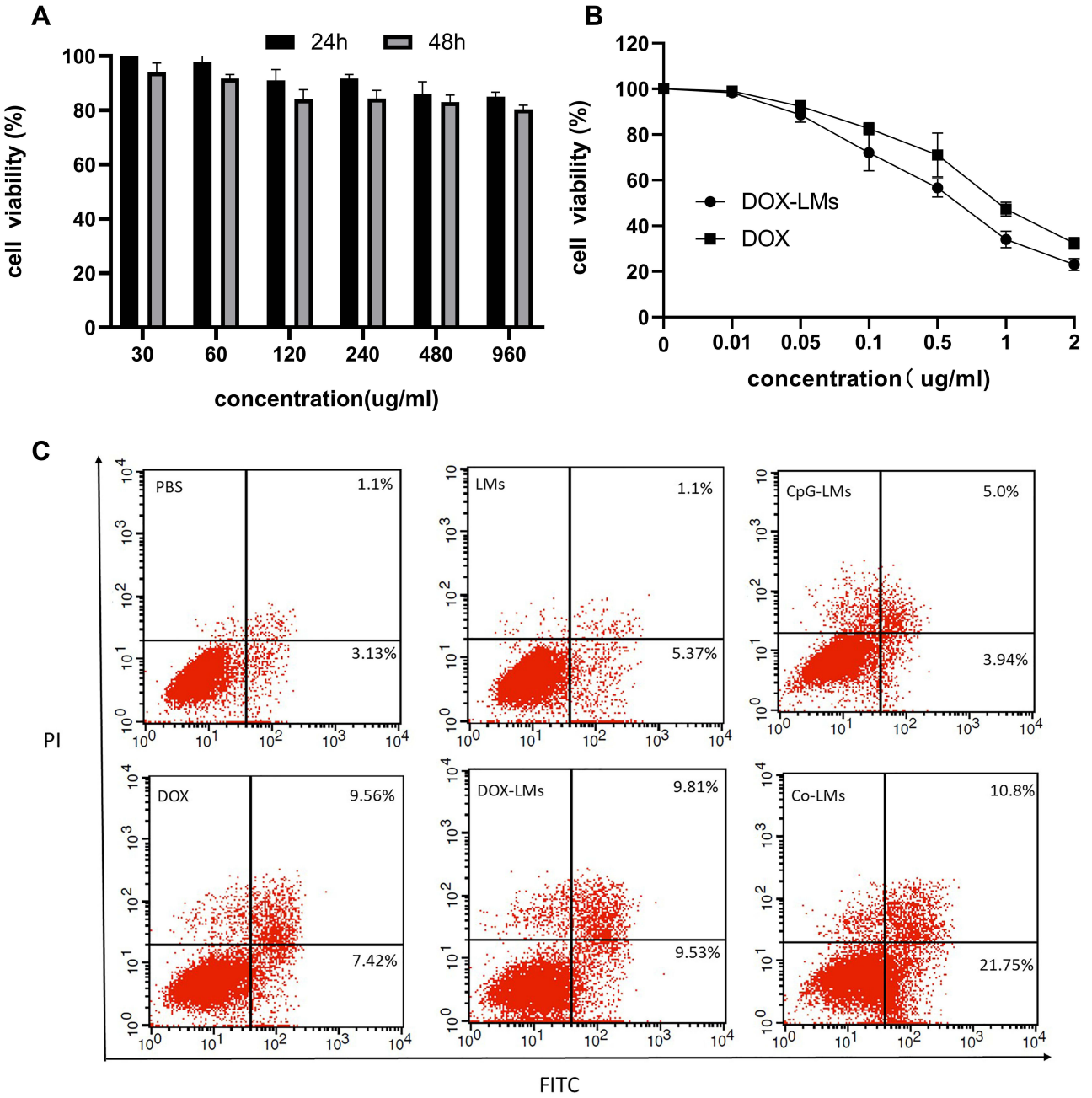

Figure 5 In vitro antitumor effect of Co-LMs. (**A**) The viability of 4T1 cells after treatment with different concentrations of blank vector (LMs) for 24h or 48h. (**B**) The IC_{50} value of DOX and DOX-LMs anti 4T1cell. (**C**) Cell apoptosis analysis of 4T1 cells measured by flow cytometry (DOX: 0.5 μg/mL,CpG:100nM). Data are expressed as the mean ± SD (n = 3).

that achieved by treatment with LMs or lipo2000-CpG (P<0.01). TNF-α and IL-6 mRNA levels were consistent with the ELISA results, indicating the potential of CpG-LMs as an immune adjuvant (Figure 6B).

In vivo Distribution and Antitumor Effects

The investigation of in vivo drug bio-distribution is essential for the evaluation of safety and effectiveness of nano delivery system. Cy5-CpG-LMs were intravenously injected via the tail vein into tumor-bearing mice. As shown in Figure 7, the organ were scanned at 30 min, 1 h, 2 h, 6 h, 12h, and 24 h post-injection, and images were obtained. The fluorescence was initially mainly distributed at the liver site, and over time, the nanoparticles began to circulate to the

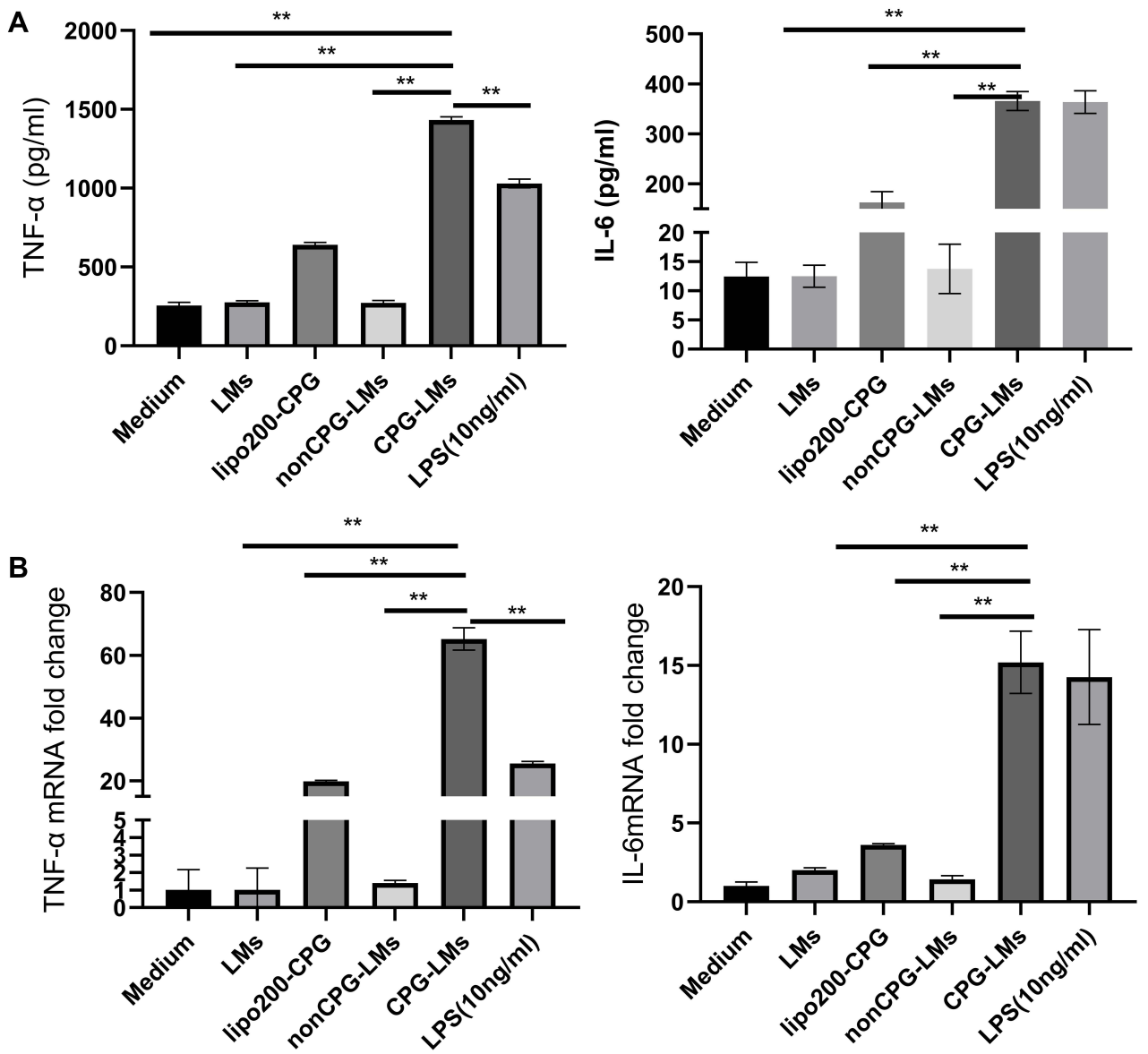

Figure 6 Immunostimulatory activity of CpG-LMs in vitro: (**A**) IL-6 production in RAW264.7 cells determined by ELISA after varies treatment for 24 h, TNF-α production in RAW264.7 cells determined by ELISA after varies treatment for 8 h. (**B**) IL-6 and TNF-α mRNA levels measured by RT-PCR. **p <0.01.

tumor site and accumulated at the tumor site. The signal intensity gradually increased, with a peak at 12 h after administration. The nanoparticles were gradually metabolized and excreted from the body. Importantly, there was no distribution in heart and lung, which indicated that our nanoparticles reduce drug's cardiac and pulmonary toxicity. This is mainly due to the nano-sized EPR effect, which enables drugs to target and remain in tumor sites. Moreover, the cross-linked disulfide bond in the nano micelles can reduce the leakage of drugs in the blood circulation to a greater extent.[30]

The antitumor effects of Co-LMs were investigated in 4T1 tumor transplantation model mice in vivo. We tested the in vivo therapeutic efficacy of PBS, LMs, CpG-LMs, DOX, DOX-LMs, and Co-LMs and the tumor volumes were monitored at regular intervals after treatment (Figure 8A). Body weight change was examined to evaluate the systemic toxicity. As shown in Figure 8B, except for DOX group, none of the treatments, resulted in a decrease in body weight, indicating that DOX-LMs, CpG-LMs, and Co-LMs did not induce significant systemic toxicity. Compared with PBS injection group, LMS injection group had negligible inhibitory effect on tumor growth. The CpG-LMs, DOX, DOX-LMs and Co-LMs injection groups demonstrated tumor inhibition at different levels. At day 21, the tumor size in the Co-LMs group was 6.8-, 5.1-, and

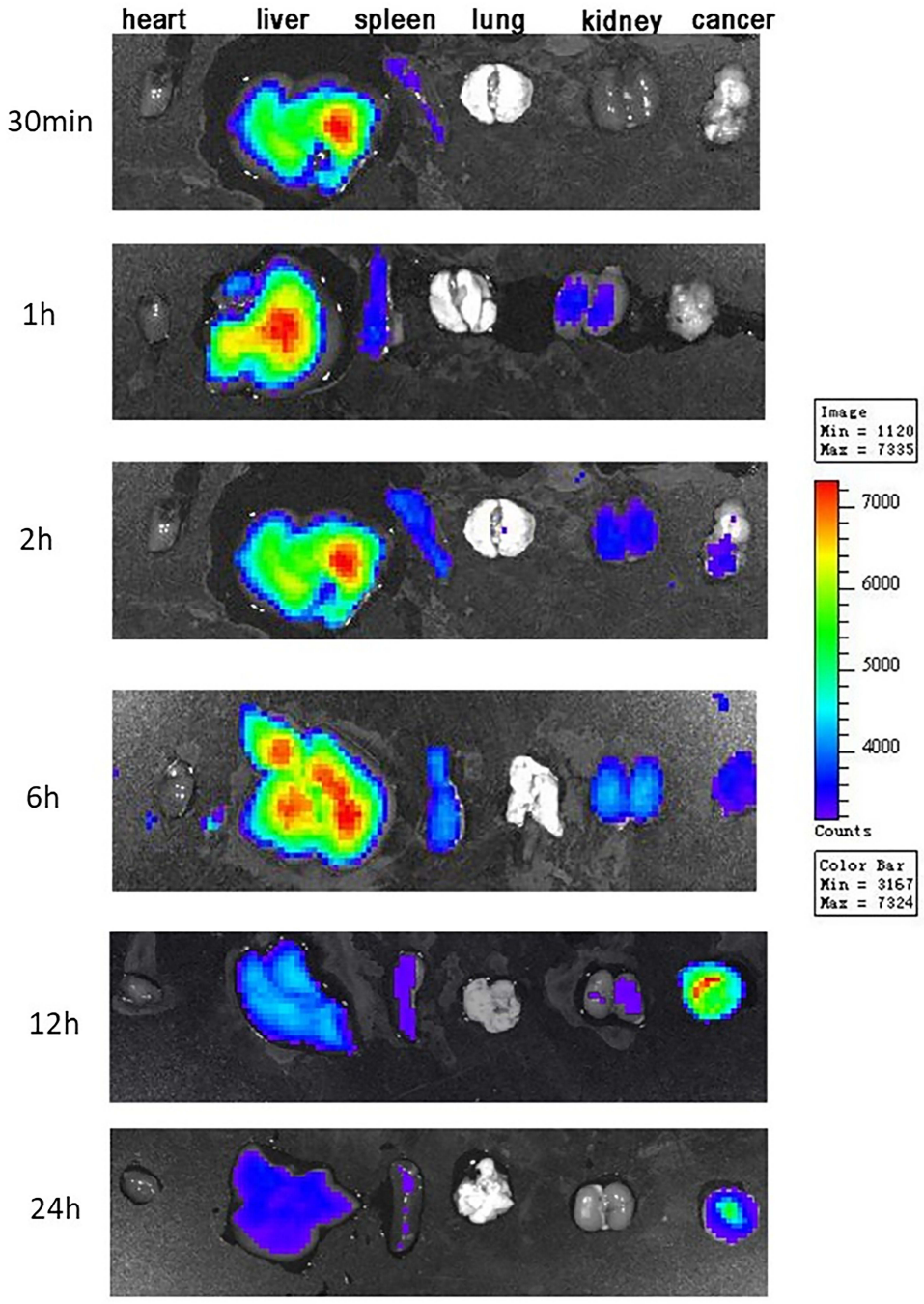

Figure 7 Ex vivo imaging of tumors and organs collected from mice administered Cy5-CpG-LMs (N/P=10) for30min, 1h, 2h, 6h, 12h and 24h (CpG: 100 nM).

2.3-fold lower than that in the LMs, CpG-LMs, and DOX-LMs group. The difference in average weight of tumors isolated on day 21 also showed the same trend (Figure 8C and D). Histological studies were performed to further study the in vivo antitumor effects. As shown in Figure 8E, the tumor showed more obvious necrotic areas in the Co-LMs group than that in the CpG-LMs, DOX and DOX-LMs groups. The above results show that the CpG-LMs group had lower treatment effect of TNBC, which indicate that only immune adjuvant is relatively difficult to generate strong anti-tumor immune response. The possible reason is that CpG is only strengthening the vitality of immune cells and cannot make immune cells accurately identify tumor cells. However, in the Co-LMs group, DOX induced apoptosis of tumor cells and the tumor associated

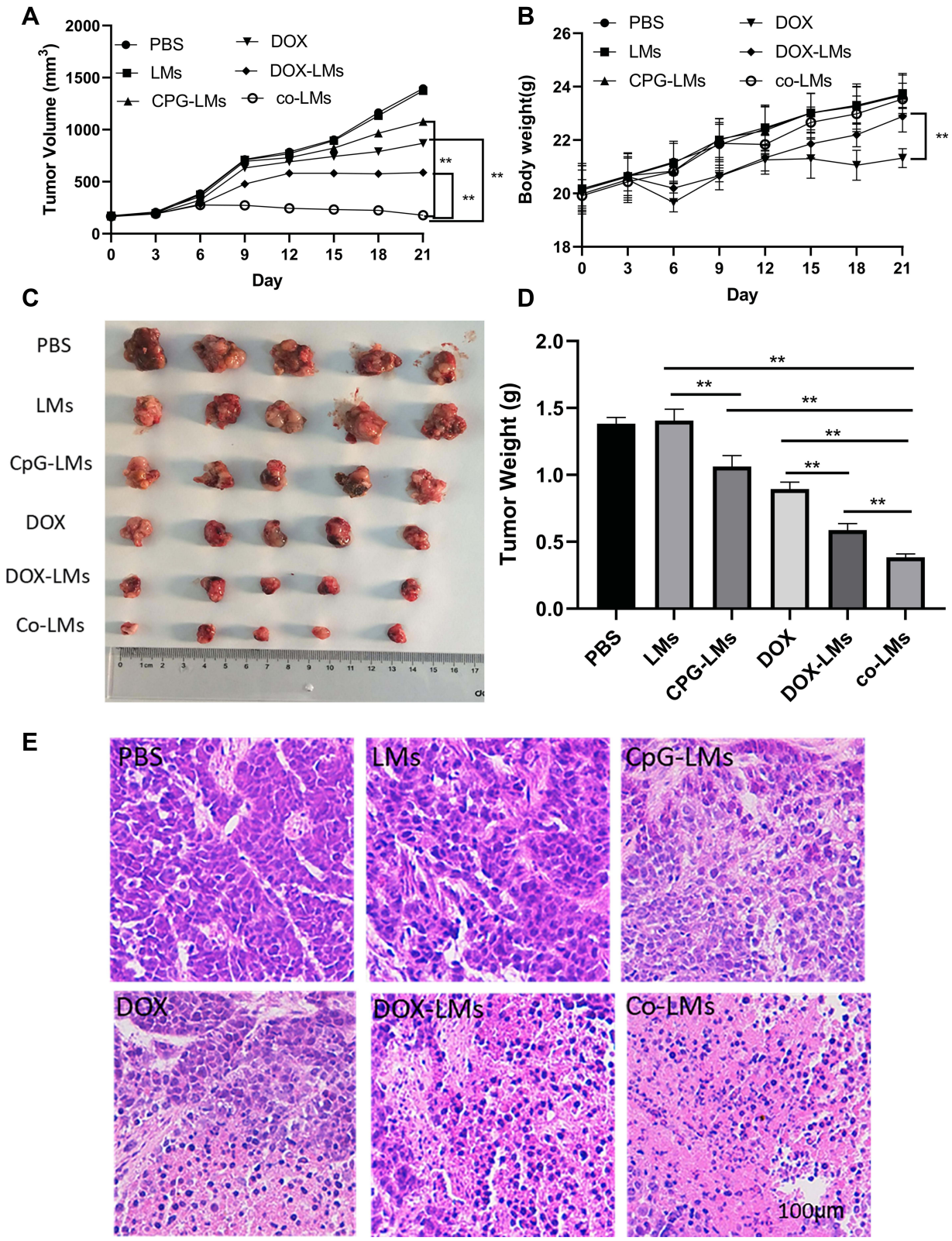

Figure 8 In vivo anti-tumor effects (**A**) Tumor growth curves of mice receiving different therapeutic regimens. (**B**) The body weight of tumor-bearing mice treated with different therapeutic regimens. (**C**) Image of excised tumor masses at the time of sacrifice after 21 days post-treatment. (**D**) The weight of the excised tumor tissues from all groups. (**E**) The histological characteristic of 4T1 tumor tissue after treatment. Data are expressed as the mean±SD (n = 5). **p <0.01, versus PBS.

antigens or "danger" signals were released, which further improved the recognition ability of the body's immune system. Therefore, Co-LMs group had a synergistic anti-tumor effect.

Detection of $CD4^+$ and $CD8^+$ T-Cell in Mice Spleen

The T-cell response to PBS, LMs, CpG-LMs, DOX, DOX-LMs and Co-LMs was measured by flow cytometry to evaluate the induced $CD4^+$ and $CD8^+$T cells, which are the two prime T cell subsets in splenocytes. As shown in Figure 9A and B, all the tested groups (LMs, CpG-LMs, DOX, DOX-LMs and Co-LMs) activated $CD4^+$ T-cells. The amount of $CD4^+$ T-cells in the mice immunized with Co-LMs (45.6%) was much higher than that in mice immunized with CpG-LMs (27.8%; $p<0.01$), LMs (7.37%; $p<0.01$) and DOX-LMs (18.2%; $p<0.01$). The production of $CD8^+$ T-cells elicited by Co-LMs (10.4%) was also higher than that induced by CpG-LMs (6.5%; $p<0.01$), LMs (3.9%; $p<0.01$) and DOX-LMs (5.6%; $p<0.01$) (Figure 9C and D). Therefore, the combined treatment of CpG and DOX effectively stimulates the tumor immune lethality in mice.

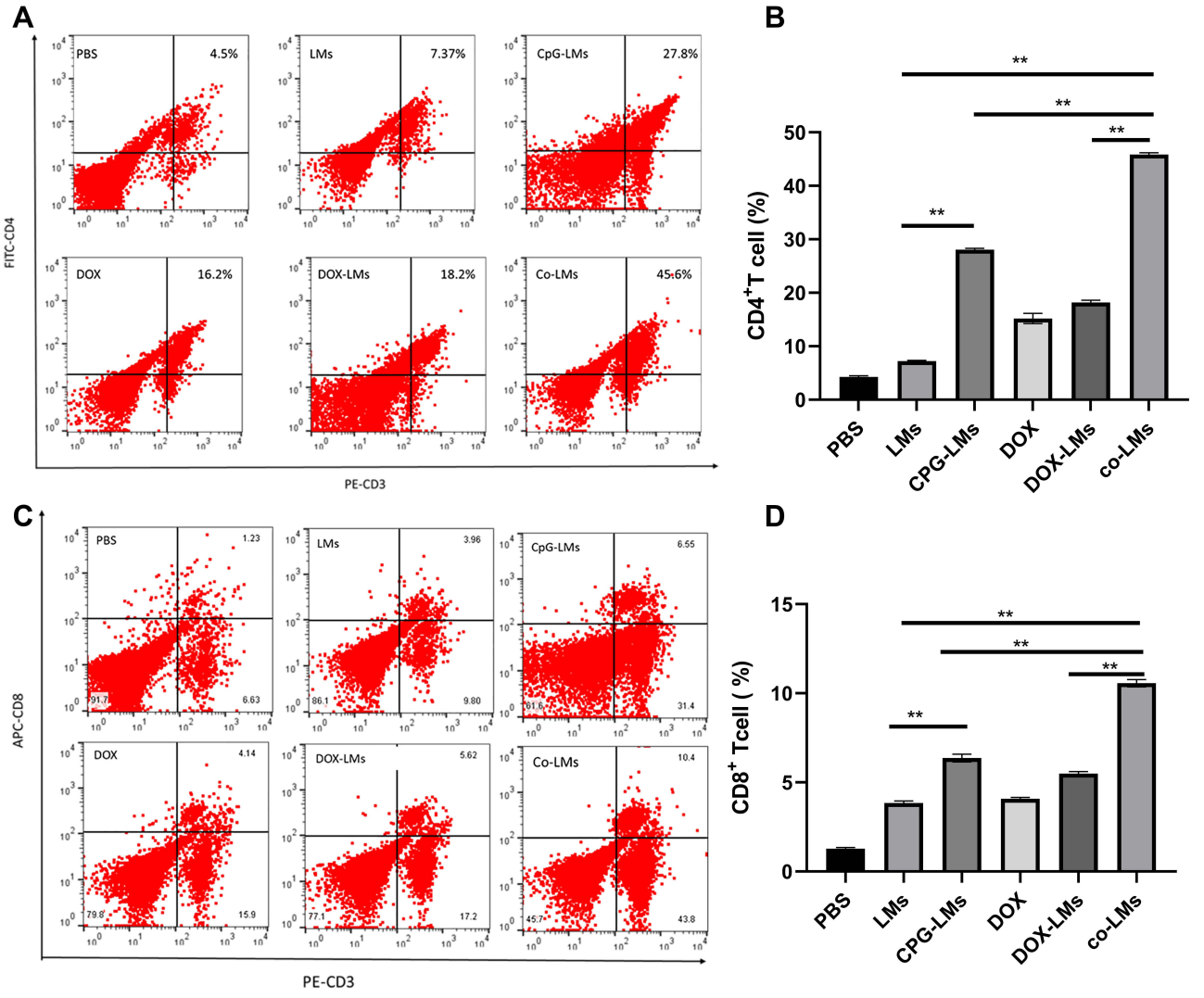

Figure 9 Induction of CD4+ and CD8+ T-cells after immune stimulation with PBS, LMs, CpG-LMs, DOX, DOX-LMs, Co-LMs. The expression of splenocyte surface molecules was determined by flow cytometry. (**A**) Representative result CD4+ T cell of independent experiments and (**B**) Quantitative analysis of the percentage of positive CD4+ T cells. (**C**) Representative result CD8+ T cell of independent experiments and (**D**) Quantitative analysis of the percentage of positive CD8+ T cells. The data shown as means±SD (n =5). The statistical significance of the results was analyzed and indicated as **p <0.01.

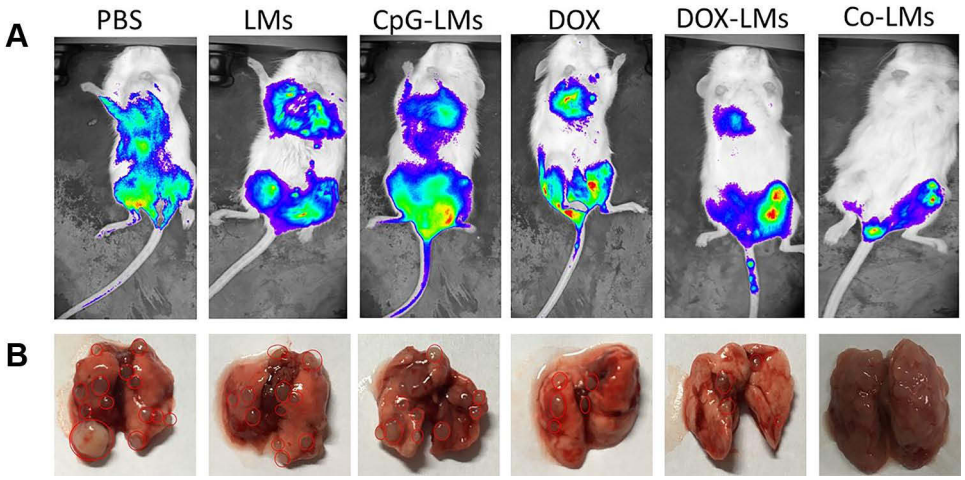

Figure 10 Inhibition of metastasis in the blood vessel metastasis. (**A**) Fluorescence intensity in mice tested 4 cycles of treatment after fuc-4T1 cells injected into the tail vein. (**B**) The dissected lung tissue after 4 cycles of treatment. Based on the total area of metastatic tumors, there were differences among the groups. *p <0.05, CpG-LMs vs PBS/LMs, **p <0.01,Co-LMs vs CpG-LMs.

Inhibition of Lung Metastasis in the Blood Vessel Metastasis

To evaluate whether Co-LMs could prevent tumor metastasis in late stage breast cancer, when a certain amount of circulating tumor cells have already invaded the blood vessels, a 4T1 bloodstream metastasis model was constructed. As shown in Figure 10A, after four cycles of treatment, each group of mice had lower limb transfer, and almost all mice were unable to move their lower limbs at the end of the experiment. This may be from the accumulation of tumor cells by tail vein injection. Importantly, there was no fluorescence accumulation in the thoracic cavity in the Co-LMs group, indicating that the nanoparticles can resist the possibility of lung metastasis of advanced breast cancer. Analyses of dissected lung tissue further confirmed this result (Figure 10B). This result may be due to the fact that chemo-immunotherapy induces the strongest memory T-cell response and provides better protection against reinfection.[23]

Conclusion

In this study, we synthesized unique nanoparticles co-loaded with DOX and CpG by self-assembly. The nanomicelle uses a cationic carrier micellar chain with arginine-histidine-lipoics acid (LH_3R_6) to link CpG oligonucleotides. We used arginine 6 (R_6) as an intracellular delivery vector for the cell penetrating peptide to synergically condense nucleotide through electrostatic interactions.[37,38] Histidine helps nanomicelles escape from endosomes through the proton sponge effect.[33,39] DOX-EMCH is a 6-maleimidocaproylhydrazone DOX derivative with a hydrazone bond that can break at pH sensitivity in the tumor microenvironment.[34,40] The nanoparticles targeted transport doxorubicin and immune adjuvants to the tumor and realize the pH and redox-sensitive of the tumor microenvironment cleavage to release drugs. Importantly, the nanoparticles reduced the leakage of doxorubicin in the blood circulation to a great extent and helped CpG escape from lysosomes. The nanoparticles were confirmed to have good anti-TNBC effects in vitro and in vivo and stimulate the tumor immune lethality of mice. More critically, the nanoparticles showed good killing effects and anti-metastatic effects on tumor cells in the blood circulation. Our research shows that for TNBC, an immune "cold tumor", chemotherapy drugs can be combined with immune activating drugs to achieve a good antitumor effect. Our results demonstrated that the synthesized nanoparticle is a smart multifunctional potential antitumor drug.

Author Contributions

All authors made a significant contribution to the work reported, whether that is in the conception, study design, execution, acquisition of data, analysis and interpretation, or in all these areas; took part in drafting, revising or critically reviewing the article; gave final approval of the version to be published; have agreed on the journal to which the article has been submitted; and agree to be accountable for all aspects of the work.

Ethics Approval

Animal experiments were approved by the Second Military Medical University ethics Committee. All animals were operated in accordance with the Guidelines for The Care and Use of Experimental Animals of Second Military Medical University.

Funding

This work was funded by the National Natural Science Foundation of China (Nos. NSFC81972891); the Science and Technology Project of Jiaxing, Zhejiang, China (Grants 2019AY32013); the Research Fund for Academician Lin He New Medicine (Grants199331309) and the Foundation of Shanghai Pharmaceutical Association.

Disclosure

The authors declare no competing interest in this work.

References

1. Sung H, Ferlay J, Siegel RL, et al. Global cancer statistics 2020: GLOBOCAN estimates of incidence and mortality worldwide for 36 cancers in 185 countries. *CA Cancer J Clin*. 2021;71(3):209–249. doi:10.3322/caac.21660
2. Cancello G, Bagnardi V, Sangalli C, et al. Phase II study with epirubicin, cisplatin, and infusional fluorouracil followed by weekly paclitaxel with metronomic cyclophosphamide as a preoperative treatment of triple-negative breast cancer. *Clin Breast Cancer*. 2015;15(4):259–265. doi:10.1016/j.clbc.2015.03.002
3. Gong C, Tian J, Wang Z, et al. Functional exosome-mediated co-delivery of doxorubicin and hydrophobically modified microRNA 159 for triple-negative breast cancer therapy. *J Nanobiotechnology*. 2019;17(1):93. doi:10.1186/s12951-019-0526-7
4. Noguchi E, Shien T, Iwata H. Current status of PD-1/PD-L1 blockade immunotherapy in breast cancer. *Jpn J Clin Oncol*. 2021;51(3):321–332. doi:10.1093/jjco/hyaa230
5. Fan W, Yung B, Huang P, et al. Nanotechnology for multimodal synergistic cancer therapy. *Chem Rev*. 2017;117(22):13566–13638. doi:10.1021/acs.chemrev.7b00258
6. Melero I, Berman DM, Aznar MA, et al. Evolving synergistic combinations of targeted immunotherapies to combat cancer. *Nat Rev Cancer*. 2015;15(8):457–472. doi:10.1038/nrc3973
7. Palmer AC, Sorger PK. Combination cancer therapy can confer benefit via patient-to-patient variability without drug additivity or synergy. *Cell*. 2017;171(7):1678–1691. doi:10.1016/j.cell.2017.11.009
8. Peng J, Xiao Y, Li W, et al. Photosensitizer micelles together with IDO inhibitor enhance cancer photothermal therapy and immunotherapy. *Adv Sci*. 2018;5(5):1700891. doi:10.1002/advs.201700891
9. Robert C, Long GV, Brady B, et al. Nivolumab in previously untreated melanoma without BRAF mutation. *N Engl J Med*. 2015;372(4):320–330. doi:10.1056/NEJMoa1412082
10. Winer Eric P, Lipatov O, Im S-A, et al. Pembrolizumab versus investigator-choice chemotherapy for metastatic triple-negative breast cancer (KEYNOTE-119): a randomised, open-label, phase 3 trial.. *Lancet Oncol*. 2021;22(4):499–511. doi:10.1016/S1470-2045(20)30754-3
11. Labani-Motlagh A, Ashja-Mahdavi M, Loskog A. The tumor microenvironment: a milieu hindering and obstructing antitumor immune responses. *Front Immunol*. 2020;11:940. doi:10.3389/fimmu.2020.00940
12. Retecki K, Seweryn M, Graczyk-Jarzynka A, et al. The immune landscape of breast cancer: strategies for overcoming immunotherapy resistance. *Cancers*. 2021;13(23):6012. doi:10.3390/cancers13236012
13. Xia Q, Gong C, Gu F, et al. Functionalized multi-walled carbon nanotubes for targeting delivery of immunostimulatory CpG oligonucleotides against prostate cancer. *J Biomed Nanotechnol*. 2018;14(9):1613–1626. doi:10.1166/jbn.2018.2605
14. Mastria EM, Cai LY, Kan MJ, et al. Nanoparticle formulation improves doxorubicin efficacy by enhancing host antitumor immunity. *J Control Release*. 2018;269:364–373. doi:10.1016/j.jconrel.2017.11.021
15. Deng C, Zhang Q, Jia M, et al. Tumors and their microenvironment dual-targeting chemotherapy with local immune adjuvant therapy for effective antitumor immunity against breast cancer. *Adv Sci*. 2019;6(6):1801–1868. doi:10.1002/advs.201801868
16. Song Q, Yin Y, Shang L, et al. Tumor microenvironment responsive nanogel for the combinatorial antitumor effect of chemotherapy and immunotherapy. *Nano Lett*. 2017;17(10):6366–6375. doi:10.1021/acs.nanolett.7b03186
17. Feng B, Zhou F, Hou B, et al. Binary cooperative prodrug nanoparticles improve immunotherapy by synergistically modulating immune tumor microenvironment. *Adv Mater*. 2018;30(38):1803001. doi:10.1002/adma.201803001
18. Emens LA, Middleton G. The interplay of immunotherapy and chemotherapy: harnessing potential synergies. *Cancer Immunol Res*. 2015;3(5):436–443. doi:10.1158/2326-6066.CIR-15-0064
19. Lu J, Liu X, Liao YP, et al. Breast cancer chemo- immunotherapy through liposomal delivery of an immunogenic cell death stimulus plus interference in the IDO-1 pathway. *ACS nano*. 2018;12:11041–11061.
20. Tarantino P, Gandini S, Trapani D, et al. Immunotherapy addition to neoadjuvant chemotherapy for early triple negative breast cancer: a systematic review and meta-analysis of randomized clinical trials. *Crit Rev Oncol Hematol*. 2021;159:103223. doi:10.1016/j.critrevonc.2021.103223
21. Judd J, Borghaei H. Combining immunotherapy and chemotherapy for non–small cell lung cancer. *Thorac Surg Clin*. 2020;30(2):199–206. doi:10.1016/j.thorsurg.2020.01.006
22. Jagieła J, Bartnicki P, Rysz J. Nephrotoxicity as a complication of chemotherapy and immunotherapy in the treatment of colorectal cancer, melanoma and non-small cell lung cancer. *Int J Mol Sci*. 2021;22(9):4618. doi:10.3390/ijms22094618
23. Dong X, Yang A, Bai Y, et al. Dual fluorescence imaging-guided programmed delivery of doxorubicin and CpG nanoparticles to modulate tumor microenvironment for effective chemo-immunotherapy. *Biomaterials*. 2020;230:119659. doi:10.1016/j.biomaterials.2019.119659

24. Wu J, Waxman DJ. Immunogenic chemotherapy: dose and schedule dependence and combination with immunotherapy. *Cancer Lett*. 2018;419:210–221. doi:10.1016/j.canlet.2018.01.050
25. Wang C, Sun W, Wright G, et al. Inflammation-triggered cancer immunotherapy by programmed delivery of CpG and Anti-PD1 antibody. *Adv Mater*. 2016;28(40):8912–8920. doi:10.1002/adma.201506312
26. Zhu G, Lynn GM, Jacobson O, et al. Albumin/vaccine nanocomplexes that assemble in vivo for combination cancer immunotherapy. *Nat Commun*. 1954;2017(8):3.
27. Chan KH, Tay JJJ. Advancement of peptide nanobiotechnology via emerging microfluidics technology. *Micromachines*. 2019;10:627.
28. Chan KH, Lee WH, Ni M, Loo Y, Hauser CAE. C-Terminal residue of ultrashort peptides impacts on molecular self-assembly, hydrogelation, and interaction with small-molecule drugs. *Sci Rep*. 2018;8(1):17127. doi:10.1038/s41598-018-35431-2
29. Gong C, Hu C, Gu F, et al. Co-delivery of autophagy inhibitor ATG7 siRNA and docetaxel for breast cancer treatment.. *J Control Release*. 2017;266:272–286. doi:10.1016/j.jconrel.2017.09.042
30. Yao C, Liu J, Wu X, et al. Reducible self-assembling cationic polypeptide-based micelles mediate co-delivery of doxorubicin and microRNA-34a for androgen-independent prostate cancer therapy.. *J Control Release*. 2016;232:203–214. doi:10.1016/j.jconrel.2016.04.034
31. Hu C, Gu F, Tai Z, et al. Synergistic effect of reduced polypeptide micelle for co-delivery of doxorubicin and TRAIL against drug-resistance in breast cancer. *Oncotarget*. 2016;7:38.
32. Hu C, Gu F, Gong C, et al. Co-delivery of the autophagy inhibitor si-Beclin1 and the doxorubicin nano-delivery system for advanced prostate cancer treatment. *J Biomater Appl*. 2022;36(7):1317–1331. doi:10.1177/08853282211060252
33. Midoux P, Pichon C, Yaouanc JJ, et al. Chemical vectors for gene delivery: a current review on polymers, peptides and lipids containing histidine or imidazole as nucleic acids carriers. *Br J Pharmacol*. 2009;157(2):166–178. doi:10.1111/j.1476-5381.2009.00288.x
34. Acharya S, Sahoo SK. PLGA nanoparticles containing various anticancer agents and tumour delivery by EPR effect. *Adv Drug Deliv Rev*. 2011;63 (3):170–183. doi:10.1016/j.addr.2010.10.008
35. Yin J, Ren W, Yang G, et al. L-Cysteine metabolism and its nutritional implications. *Mol Nutr Food Res*. 2016;60(1):134–146. doi:10.1002/mnfr.201500031
36. Tian M, Guo F, Sun Y, et al. A fluorescent probe for intracellular cysteine overcoming the interference by glutathione. *Mol Nutr Food Res*. 2016;60 (1):134–146.
37. Futaki S. Membrane-permeable arginine-rich peptides and the translocation mechanisms. *Adv Drug Deliver Rev*. 2005;57(4):547–558. doi:10.1016/j.addr.2004.10.009
38. Lorents A, Sa¨a¨lik P, Langel U, et al. Arginine-rich cell-penetrating peptides require nucleolin and cholesterol-poor subdomains for translocation across membranes. *BioconjugChem*. 2018;29(4):1168–1177.
39. L¨achelt U, Kos P, Mickler FM, et al. Fine-tuning of proton sponges by precise diaminoethanes and histidines in pDNA polyplexes. *Nanomedicine*. 2014;10(1):35–44. doi:10.1016/j.nano.2013.07.008
40. Conner SD, Schmid SL. Regulated portals of entry into the cell. *Nature*. 2003;422(6927):37–44. doi:10.1038/nature01451